HYDROLOGICAL PROCESSES
Hydrol. Process. **19**, 2689–2699 (2005)
Published online 19 April 2005 in Wiley InterScience (www.interscience.wiley.com). DOI: 10.1002/hyp.5781

Measuring thaw depth beneath peat-lined arctic streams using ground-penetrating radar

John H. Bradford,[1]* James P. McNamara,[2] William Bowden[3] and Michael N. Gooseff[4]

[1] *Center for Geophysical Investigation of the Shallow Subsurface, Boise State University, Boise, ID, USA*
[2] *Department of Geosciences, Boise State University, Boise, ID, USA*
[3] *School of Natural Resources, University of Vermont, Burlington, VT, USA*
[4] *Department of Aquatic, Watershed, and Earth Resources, Utah State University, Logan, UT, USA*

Abstract:

In arctic streams, depth of thaw beneath the stream channel is likely a significant parameter controlling hyporheic zone hydrology and biogeochemical cycling. As part of an interdisciplinary study of this system, we conducted a field investigation to test the effectiveness of imaging substream permafrost using ground-penetrating radar (GPR). We investigated three sites characterized by low-energy water flow, organic material lining the streambeds, and water depths ranging from 0·2 to 2 m. We acquired data using a 200 MHz pulsed radar system with the antennas mounted in the bottom of a small rubber boat that was pulled across the stream while triggering the radar at a constant rate. We achieved excellent results at all three sites, with a clear continuous image of the permafrost boundary both peripheral to and beneath the stream. Our results demonstrate that GPR can be an effective tool for measuring substream thaw depth. Copyright © 2005 John Wiley & Sons, Ltd.

KEY WORDS ground-penetrating radar; permafrost; arctic streams; thaw bulb

INTRODUCTION

The North Slope of Alaska is underlain by thick and continuous permafrost that reaches the surface during the winter and thaws to a depth of up to 1 m in terrestrial soils by late summer. This active layer has been shown to have important controls on numerous hydrologic, geomorphologic, and ecologic processes (Hinzman *et al*., 1991; Kane *et al*., 1992; Leibman, 1995; McMichael *et al*., 1997; McNamara *et al*., 1997, 1998). However, little, if any, work has been done concerning the role of the thaw cycle under rivers and streams on biogeochemical processes. This is a significant gap in our understanding of arctic streams, because the hyporheic zone plays an important role in biogeochemical cycling. As the depth of thaw increases under a stream we might expect changes in hyporheic exchange dynamics and residence time. Because biogeochemical regeneration in hyporheic zones is likely to be an important source of nutrients in arctic streams (Edwardson, 1997; Edwardson *et al*., 2003), the seasonal expansion of the hyporheic zone and hyporheic processing should have important impacts on stream structure and function. A first step towards addressing this problem is to develop efficient, non-invasive methods to monitor the depth of thaw under arctic streams, henceforth called the thaw bulb. Through basic ground-penetrating radar (GPR) principles and a field investigation, we evaluate the feasibility of using GPR to measure the extent of the thaw bulb under streams in northern Alaska.

* Correspondence to: John H. Bradford, CGISS MG-206, Boise State University, 1910 University Dr., Boise, ID 83725, USA. E-mail: johnb@cgiss.boisestate.edu

Received 13 November 2003
Accepted 12 July 2004

PRINCIPLES OF GPR IN PERMAFROST INVESTIGATIONS

In GPR studies, the transmitting antenna generates a broad-band electric field that propagates through the subsurface and is reflected at boundaries separating materials with differing electric properties (electric permittivity, magnetic permeability, and conductivity). The reflected wavefield is measured with the receiving antenna and used to produce a reflector map that is an image of electric impedance contrasts in the subsurface. The reflector map is similar to a cross-section of the subsurface.

GPR reflections are produced primarily by contrasts in electric permittivity. The permittivity in ice is approximately $3\varepsilon_0$ and in water is approximately $80\varepsilon_0$, where ε_0 is the permittivity of free space. Thus, there is a large permittivity contrast between ice and water. A number of mixing models have been developed to relate both the sediment matrix and material filling the pore space to the bulk electric permittivity. Greaves *et al*. (1996) review several of these models. Although some variations exist, the models generally show that replacing water in the pore space with ice yields a significant decrease in electric permittivity, or equivalently an increase in radar velocity. Field observations have verified this effect and, currently, a significant body of work establishes that GPR is a tool well suited to mapping permafrost boundaries (Davis *et al*., 1976; Arcone *et al*., 1992; Doolittle *et al*., 1990, 1992; Hinkel *et al*., 2001). For example, Arcone *et al*. (1998) found that electric permittivity decreased by a factor of 4 or more at the saturated sediment–permafrost boundary. They were able to map strong reflections from the upper and lower permafrost boundaries, as well as from within the permafrost. GPR's strong sensitivity to water, and the recognition that GPR provides the highest resolution of any available surface geophysical tool, suggests that it is optimal for mapping the substream saturated sediment–permafrost interface.

Substream imaging presents a unique set of challenges that are primarily related to the strong frequency dependence of radar wave velocity and attenuation as the signal propagates through water (Figure 1). Generally, higher frequency signal components travel faster and are more strongly attenuated. This frequency dependence results in dispersion of the waveform. Dispersion presents a processing challenge, as many processing algorithms assume a constant waveform. Additionally, because higher frequency components are attenuated more strongly, the dominant frequency is shifted toward the low end of the spectrum, which results in lower resolution potential. An increase in dissolved solid concentration compounds the problem, because the signal is attenuated more strongly as the electric conductivity of the water increases.

Despite these limitations, several workers have demonstrated that GPR can be an effective tool for providing high-resolution sub-bottom images in freshwater bodies where the water has relatively low conductivity (Haeni, 1996; Powers *et al*., 1999; Versteeg *et al*., 2001; Buynevich and Fitzgerald, 2003). Although little work

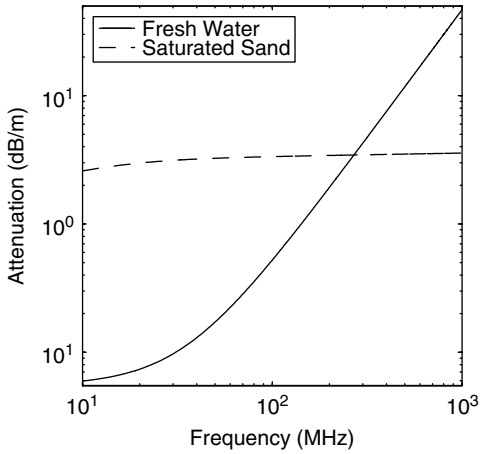

Figure 1. Attenuation curves in the GPR frequency band for fresh water and a typical water-saturated sand. Curves were computed using the Cole–Cole equations (Cole and Cole, 1941). Note the strong frequency dependence for wave propagation through water

has been published on sub-bottom GPR imaging in cold environments, several workers have demonstrated effective water-bottom imaging on cold-region water bodies (Delaney *et al*., 1990; Schwamborn *et al*., 2002). For example, Best *et al*. (2005) report using GPR to image both the ice–water contact below the frozen river surface and the water–streambed contact on the Kuparuk River, Alaska.

In a GPR profile, the recorded wavefield is a distorted picture of the subsurface. Small-scale heterogeneity results in scattering diffractions. If these heterogeneities are point-like, then the diffractions appear as hyperbolic events in a reflection profile. Further, because the angle of incidence and angle of reflection must be equal, the apparent position of a dipping reflection is not the spatial position of the subsurface boundary. The boundary dip angle is greater than the reflection dip angle, the reflection length is greater than the boundary length, and the reflection position is downdip of the boundary position (Yilmaz, 2001). Wavefield migration is a data-processing tool that seeks to place reflected energy at its point of origin; diffractions are collapsed and dipping reflections are moved to their correct spatial position. Thus, a correctly migrated reflection section is a spatially accurate image of subsurface boundaries.

Migration depends strongly on an accurate estimate of the GPR velocity distribution. And, perhaps more directly relevant to data interpretation, an accurate velocity estimate is required to compute reflector depth or layer thickness. In some cases it is possible to take advantage of wavefield scattering and the velocity dependence of migration to measure the velocity distribution using migration velocity analysis (MVA). With MVA, one first performs a series of constant-velocity migrations with a range of velocities, then picks the velocity at a given depth/horizontal position that collapses diffractions and maximizes coherence along complexly dipping reflections. The measured velocity distribution is then used to produce a migrated reflection image and to estimate reflector depth. There is an extensive body of literature that discusses a plethora of migration methods. Yilmaz (2001) gives an overview of migration theory and methods as applied to seismic reflection. To a good approximation, these methods are equally applicable to GPR.

The resolving power of the GPR system limits the minimum thaw-bulb thickness that we can measure accurately. The wavelength λ of the signal controls the resolution, with a shorter wavelength signal capable of resolving finer features. Wavelength is related to velocity v and frequency f by the simple relationship $\lambda = v/f$. It is clear from this relationship that higher frequencies result in finer resolution. However, higher frequencies are attenuated more strongly, so there is a trade off between resolution and depth of penetration. The often quoted $\lambda/4$ vertical resolution limit (Yilmaz, 2001) means that objects separated by less than this distance cannot be identified as distinct objects. This is the lower limit of our ability to measure the thickness of the thaw bulb accurately. Lateral resolution is a function of depth and is given by $\sqrt{\lambda z/2}$. In the migrated domain, the depth dependence is eliminated and the lateral resolution is approximately $\lambda/2$ (Yilmaz, 2001). The wavelength of the signal decreases with velocity, so that low velocities lead to higher resolution potential. Because the thaw bulb is comprised of water-saturated sediments, the velocity is very low, resulting in good resolution potential. Assuming a dominant frequency of 200 MHz and a velocity in water-saturated sand of 0·06 m ns^{-1}, the signal wavelength is 0·3 m and our resolution limits are roughly 0·075 m vertically and 0·15 m laterally.

FIELD SETTING

We conducted the field investigation in August, 2003, near the end of the thaw season, when we expected the thaw depth to be near its maximum. We investigated three sites located within the Kuparuk River drainage, north of the Brooks Range, Alaska (Figure 2). Two sites were located on Imnavait Creek, a small tributary of the Kuparuk River. Imnavait Creek is a beaded stream characterized by a series of small ponds connected by relatively fast-moving shallow channels. Flow in the stream is characterized generally as low energy, with a peat-lined streambed and stream banks. We acquired radar profiles across two sections of the stream: a narrow stream interval 0·91 m wide and 0·27 m deep (Site 1), and a ponded interval 12·8 m wide and 2·1 m deep (Site 2). The third site we investigated was located along an unnamed meandering stream that flows

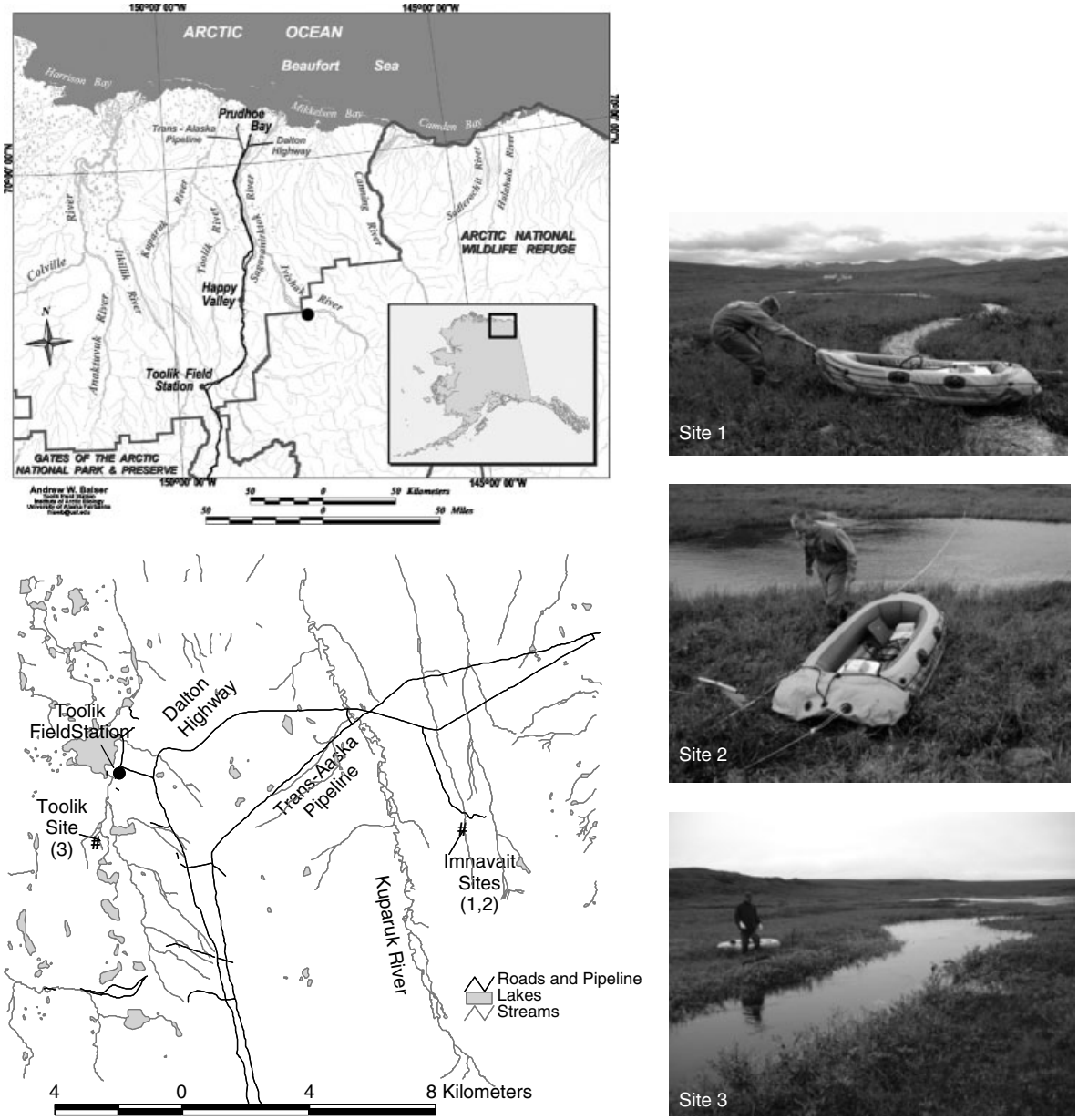

Figure 2. Location and photographs of the three study sites within the Kuparuk watershed. Maps are courtesy of Andrew Balser, Toolik GIS

into Toolik Lake (Site 3). General characteristics of this stream were similar to the Imnavait sites, but the channel morphology represents an intermediate case between the very shallow Site 1 and relatively deep Site 2. Stream width at Site 3 was 2 m and maximum water depth was 1·3 m. The stream channel cut sharply into the surficial peat and sediments with nearly vertical channel walls. Conductivity of stream waters in the study area is on the order of 20–50 μS cm^{-1}, which did not prohibit effective sub-bottom imaging with radar. A significant amount of rain accumulated during our field campaign, resulting in high water levels within the streams and fully saturated peat with some pooled water along the banks.

DATA ACQUISITION AND PROCESSING

We used a commercial pulsed radar system with 200 MHz antennas and high-power transmitter (1000 V) to maximize penetration beneath the streambed. The antennas and GPR control equipment were placed in the bottom of a small rubber boat, then pulled steadily across the stream and banks on either side while triggering the radar at a constant rate. This configuration resulted in the control equipment being within 1 m of the antennas during acquisition. Although we generally tried to maintain a minimum of 5 m separation between the antennas and control equipment, a separation of only 1 m did not prohibit acquisition of high-quality data in this case. While acquiring data, we were careful to maintain a steady pull rate while minimizing downstream drift. Maintaining spatial control is critical for both interpretation and application of spatial processing operators such as migration. Additional details of GPR data acquisition are listed in Table I. In addition to acquiring the radar profiles, we measured depth to permafrost on the stream banks and shallow ($<0{\cdot}5$ m) margins of the streams by pressing a metal probe through the active layer to the point of refusal.

Except where noted otherwise, we applied the following processing flow to each dataset:

1. Time-zero correction with first break correlation to remove start of record delay and system drift.
2. DC shift and bandpass filtering with a 25–50–400–800 MHz Ormsby filter to attenuate the low-frequency transient and high-frequency random noise.
3. Background noise removal at recording times less than 30 ns by subtracting the average trace with the average trace muted below 30 ns.
4. Amplitude correction consisting of scaling by t^2 and an exponential gain correction of $22{\cdot}5$ dB μs^{-1} ($\sim 0{\cdot}5$ dB m^{-1}).
5. Frequency-wavenumber constant-velocity MVA (Stolt, 1978) to estimate thaw bulb velocity followed by conversion to interval velocities using Dix inversion (Dix, 1955).
6. Kirchhoff depth migration coupled with iterative velocity model refinement (Yilmaz, 2001).
7. Synthetic data generation using a finite difference algorithm with the migration velocity model, followed by comparison with field GPR data to verify model kinematics.

The first four steps are essentially preprocessing for migration, which result in significantly reduced noise levels and balanced data amplitudes (Figure 3). MVA and depth migration imaging with velocity model refinement (steps 5 and 6) result in two outputs: (1) a depth image of the GPR data with accurate spatial positioning of the reflections; (2) a migration velocity model that is a map of subsurface electromagnetic velocities. These two outputs are the basis for interpreting material property boundaries and provide some indication of material composition. As with most forms of geophysical data, the velocity model derived is non-unique; other velocity combinations may produce a comparable migration result. However, by incorporating known subsurface information (such as the electromagnetic wave velocity in water) and permafrost depth control points, we can minimize the uncertainty in the resulting model. Additionally, we can say that the *average migration velocity* model between any two reflectors is an accurate representation of the *average*

Table I. Acquisition parameters at all sites

System	Sensors & Software PE100A
Transmitter	1000 V
Antennas	200 MHz
Stacks/trace	8
Trace acquisition rate	0.2 s
Sampling rate	0.4 ns
Recording time	400 ns
Nominal trace spacing	10 cm

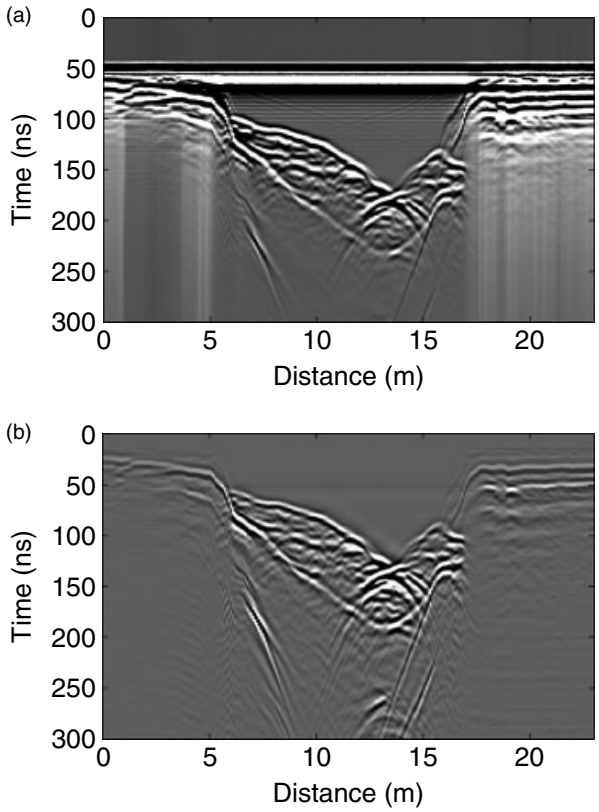

Figure 3. (a) Raw field data from Site 2, and (b) the same data after the first four stages of processing. Noise levels are signficantly reduced, the direct air and surface coupled wave are removed, and amplitudes are balanced with increasing time

actual velocity. Another tool for constraining the subsurface model is generating synthetic data using the migration velocity model (step 7). The synthetic data provide a basis for qualitative or semi-quantitative comparison with the field data, where we look for significant travel-time deviations and relative amplitude variations along a reflection.

For velocity model constraints, we estimated the active layer velocity on the stream banks by dividing the measured depth to permafrost by the interpreted radar travel-time. Within the water-filled channels we used the velocity of water at 0 °C (0·032 m ns^{-1}). Actual stream temperature varied from about 1 to 5 °C, but this variation results in a maximum change in velocity from the 0 °C value of less than 1%, which is not significant. For modelling we used a fourth-order finite difference simulation of the scalar wave equation that is available with Promax™ processing software. In using this model we are assuming frequency-independent material properties, zero electric conductivity, and uniform antenna directivity. Although these assumptions are not strictly valid and not appropriate for detailed amplitude or spectral analysis, the model does provide a useful approximation for evaluating wavefield kinematics.

RESULTS

Imnavait Creek (Sites 1 and 2)

At Site 1 (Figure 4) and Site 2 (Figure 5), we recorded a strong, continuous reflection from the permafrost boundary both peripheral to and below the channel bed. As expected, we observed significant attenuation

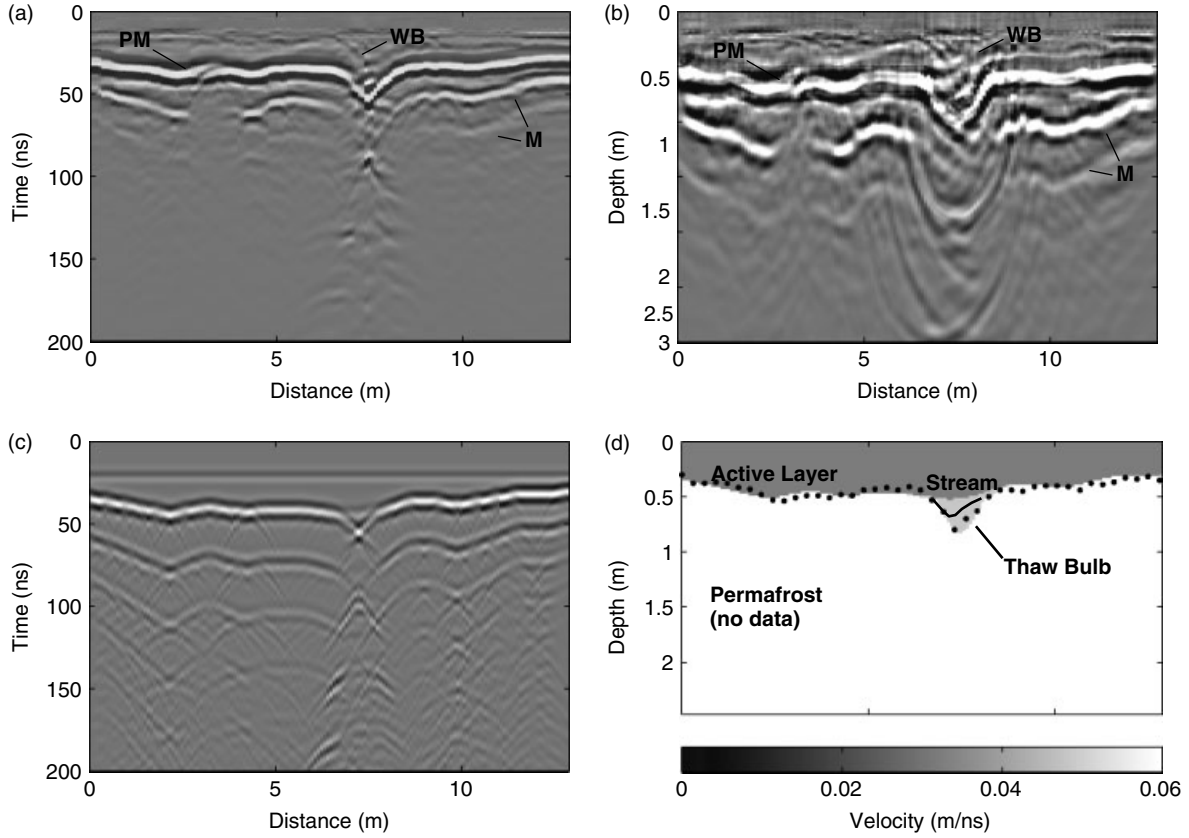

Figure 4. (a) Preprocessed data from Site 1, (b) depth-migrated image, (c) synthetic data generated using the migration velocity model, and (d) migration velocity model. There is excellent correlation between probe-measured permafrost depth and GPR-measured permafrost depth with a standard deviation of ±4 cm. (———) interpreted water bottom, (●) permafrost depth measured using a metal probe, (PM) permafrost reflection, (WB) water-bottom reflection, (M) permafrost multiple

at the high end of the frequency spectrum for the water-bottom and sub-bottom reflections (Figure 6) due to signal propagation through water. Note that there is an additional spectral shift toward lower frequencies due to antenna coupling with the water or water-saturated peat surface. As a result, the dominant frequency for water-bottom and sub-bottom reflections is on the order of 80–120 MHz (Figure 6) with corresponding wavelengths of approximately 0·5–0·3 m. Despite the shift in signal spectrum, the thaw bulb was well resolved in both profiles. At both locations we record a relatively weak water-bottom reflection, indicating a small permittivity contrast between the water and organic material lining the channel.

Some wavelet distortion was evident, but this was insignificant and standard migration algorithms produced good results (Figures 4 and 5). We observed high-amplitude permafrost multiples, which were particularly prevalent beneath the banks. The Kirchhoff algorithm we used is not designed to treat multiples properly, resulting in significant migration artifacts. However, this is of little concern, as the multiples arrive later than the permafrost reflection and are not within the zone of investigation.

Surprisingly, we found the velocity through the water-saturated peat on the streambanks to be approximately equal to that in fresh water (0·032 m ns^{-1}). Slater and Reeve (2002) reported peat velocities as low as 0·038 m ns^{-1} and Theimer *et al.* (1994) found velocities as low as 0·036 m ns^{-1}, so our measured value of 0·032 m ns^{-1} is not unrealistic. At both locations, we found slightly higher radar velocities beneath the streambed (0·049 m ns^{-1}), which is likely due to a higher concentration of inorganic material resulting

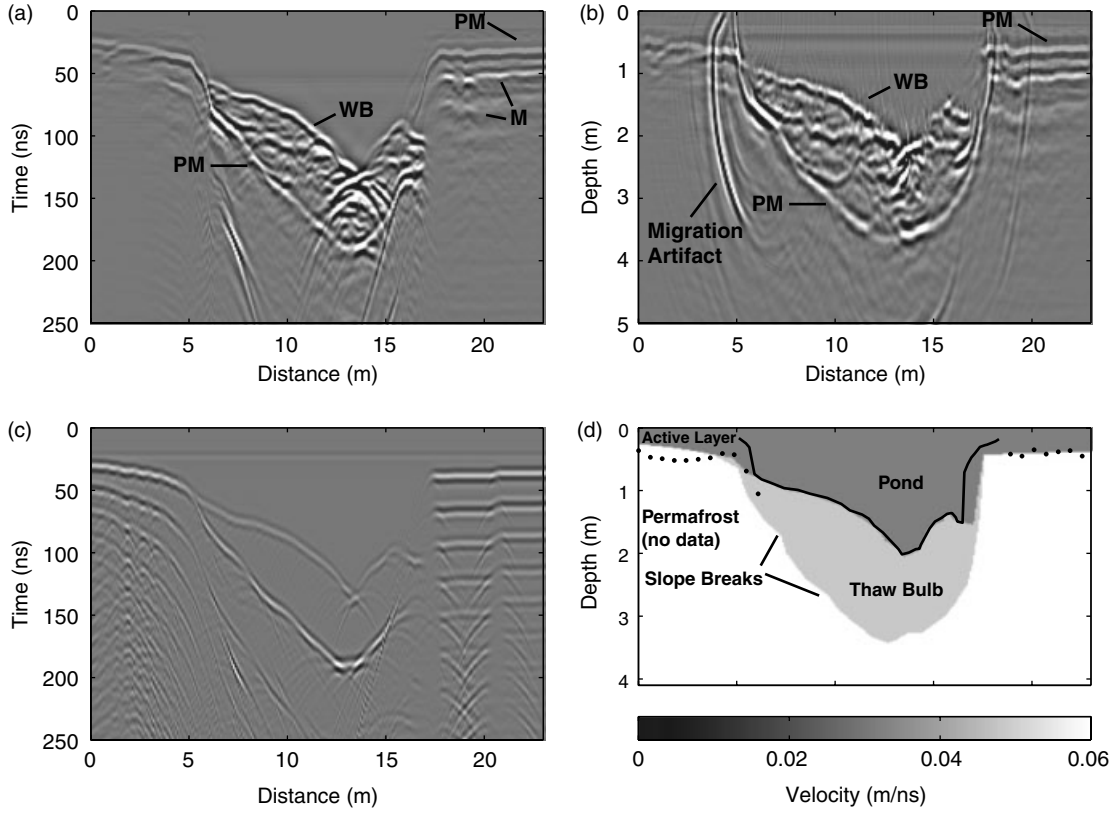

Figure 5. (a) Preprocessed data from Site 2, (b) depth-migrated image, (c) synthetic data generated using the migration velocity model, and (d) migration velocity model. Note the slope breaks along the permafrost boundary that correlate with substream stratigraphic boundaries. (———) interpreted water bottom, (●) permafrost depth using a metal probe, (PM) permafrost reflection, (WB) water-bottom reflection, (M) permafrost multiple

in lower bulk water content. No scattering was evident below the permafrost reflection, so we had no means of measuring the permafrost velocity directly. Therefore, for modelling, permafrost velocity was set at 0·15 m ns^{-1} which is within the range of values reported in the literature (Arcone *et al.*, 1998). Using measured velocities for the thaw bulb and assumed velocities for permafrost and stream water, the reflection coefficients are 0·2 and 0·5 for the water-bottom and permafrost reflections respectively. This difference in reflection coefficients is qualitatively consistent with the observed reflection amplitudes. At both sites, synthetic data, generated using the migration velocities and assumed permafrost velocity, are consistent with the field GPR data (Figures 4c and 5c).

We observed no reflections beneath the high-amplitude permafrost reflection. We found this surprising given that a significant amount of signal energy reaches the permafrost and that the permafrost is a relatively low-loss material. It is likely that impedance contrasts within the permafrost are much smaller than the water–water-bottom contrast and active layer–permafrost contrast. It is possible that high-amplitude multiples generated at these surfaces mask deeper reflections.

Owing to the shallow water depth along the Site 1 profile (Figure 4), we were able to measure both the depth to permafrost and water depth every 0·3 m across the entire profile using the metal probe. We found excellent correlation between the depth to permafrost interpreted from the radar data and the probe-measured depth with a standard deviation of ±0·04 m (Figure 4b and d). Contributing to this discrepancy was small-scale irregularity at the peat surface on the order of ±0·05 m. Acquiring GPR data from the ∼2 m long

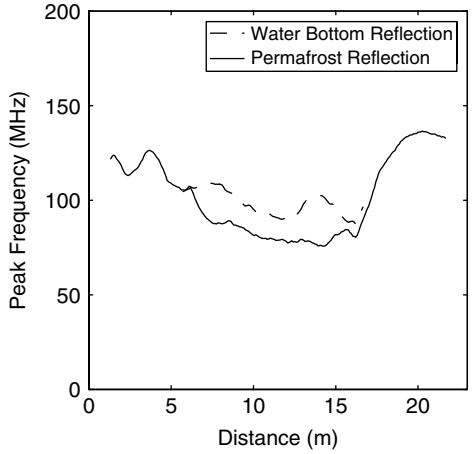

Figure 6. Dominant frequency of the water-bottom and permafrost reflections for Site 2. A 30-point smoothing filter was applied to the data. There is significant drop in frequency content as the signal passes through the pond water. This is expected given the strong frequency dependence of signal propagation through water (Figure 1)

boat provided a uniform platform that was insensitive to small-scale surface irregularity, whereas the point probe measurements included this variability. Maximum thaw-bulb thickness beneath the shallow stream was 0·53 m. This was only slightly greater than the average active layer thickness of 0·43 m measured on the banks, and is less than the 0·54 m maximum thickness measured on the bank.

A significantly thicker thaw bulb was present beneath the Site 2 profile, with a maximum thickness of 1·8 m (Figure 5). Along this profile, we measured permafrost depth every 0·6 m along the banks and at the shallow margins of the pond. Correlation with measured permafrost depth was poorer than that along the stream profile with a standard deviation of $\pm$0·15 m (Figure 5b and d). This error is primarily at the bank–water transition at 4·9 m along the profile. The most likely source for this relatively large deviation is irregular trace spacing due to a variable pull rate in making the transition from the bank to the water during data acquisition. A second potential source of error is velocity heterogeneity along the bank that is not resolved in our migration velocity model.

Of particular interest in the Site 2 profile are the slope breaks in the permafrost surface at stratigraphic boundaries (Figure 5). We speculate that these irregularities are caused by variable rates of heat transfer within different lithologies, but this interpretation has not been verified.

Toolik Lake inlet stream (Site 3)

Characteristics in the radar data from Site 3 were similar to those found at the Imnavait sites: a strong continuous reflection from the permafrost and a weaker reflection from the streambed (Figure 7). Depth migration reveals a detailed image of the permafrost boundary (Figure 7b). We recorded probe measurements at two locations and found a maximum deviation between the probe- and GPR-measured depths of 0·02 m (Figure 7b and d). This level of error is consistent with the good correlation found at Site 1. To produce good migration results we found it necessary to include a positive vertical velocity gradient within the thaw bulb that varied from at a depth of 0·5 m to at a depth of 1·9 m. This velocity profile is consistent with lithology grading from saturated peat to water-saturated sand/gravel. Thaw-bulb thickness beneath this stream was 0·61 m; this was substantially thicker than the active layer along the banks, which had a maximum thickness of 0·50 m. Again, synthetic data generated using the migration velocity model are consistent with the field data (Figure 7c).

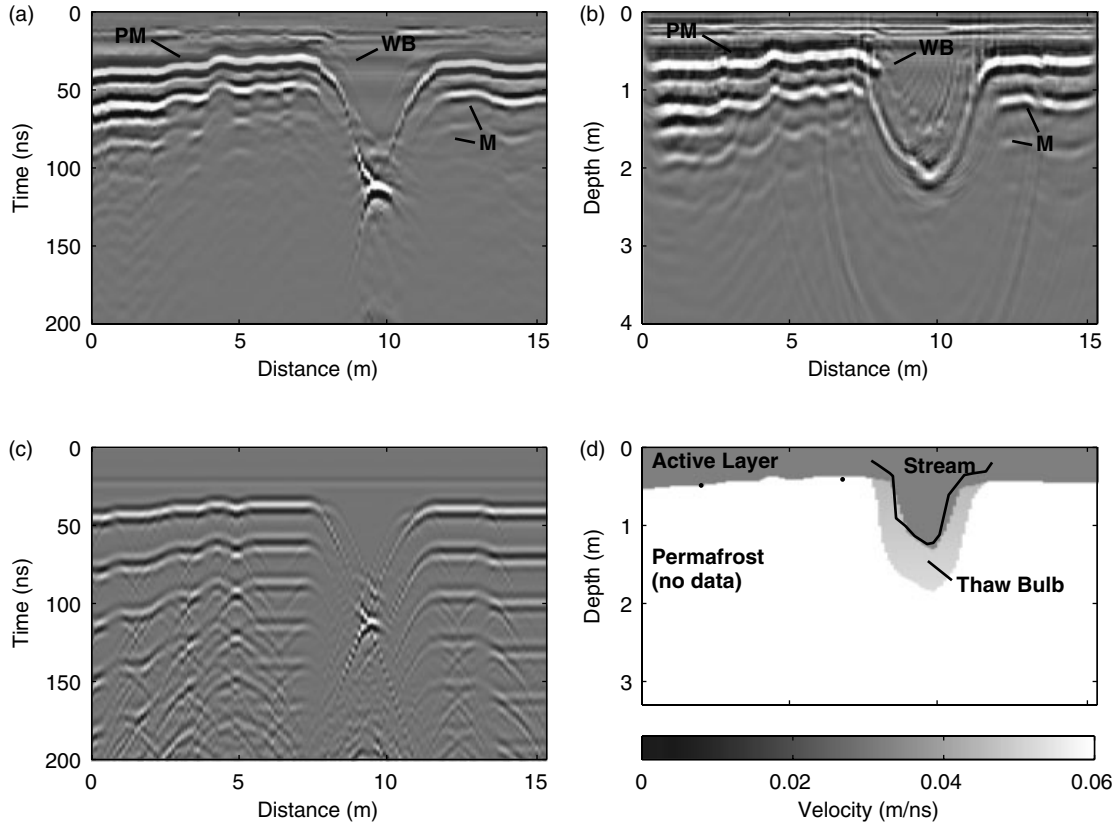

Figure 7. (a) Preprocessed data from Site 3, (b) depth-migrated image, (c) synthetic data generated using the migration velocity model, and (d) migration velocity model. There is a significant positive vertical velocity gradient within the thaw bulb that is consistent with lithology grading from primarily water-saturated organic material to water-saturated sand/gravel. (———) interpreted water bottom, (●) permafrost depth measured with a metal probe, (PM) permafrost reflection, (WB) water-bottom reflection, (M) permafrost multiple

CONCLUSIONS

Although we observed increasing thaw-bulb thickness with increasing stream depth, the reasons for this correlation are not clear, as many factors likely influence the depth of thaw. These factors include permeability of the hyporheic zone, flow rate in the channel, water depth, and solar heat input, both locally and upstream. Note that although the greatest thaw-bulb thickness was observed beneath the deepest channel (Site 2), this was also a ponded area and, therefore, had the lowest flow rate of the three sites.

Our results demonstrate that GPR can be an excellent tool for imaging the thaw bulb beneath arctic streams. Early in the thaw season, when thaw bulb thickness may only be on the order of a few centimetres, resolution will be more difficult. To improve resolution, it will be necessary to use higher frequency radar antennas. Given the low conductivity of the stream waters in our field area and the good signal penetration observed in this study, we believe that sub-bottom imaging will be possible with 400 MHz antennas or higher. It is important to note that the general characteristics at the three sites were similar: low-energy flow with relatively smooth, peat-lined streambeds. In high-energy streams (i.e. high flow rates with cobble/gravel-lined beds) the complexity of the streambed and its substrate will make radar analysis more difficult and is likely to impact the geometry of the thaw bulb. Additional testing and analysis are necessary to evaluate the efficacy of the GPR method in streams with differing flow characteristics and morphology.

ACKNOWLEDGEMENTS

This work was funded by the National Science Foundation (OPP #0327440) and conducted at Toolik Field Station operated by the University of Alaska, Fairbanks.

REFERENCES

Arcone SA, Chacho Jr EF, Delaney AJ. 1992. Short-pulse radar detection of groundwater in the Sagavanirktok River floodplain in early spring. *Water Resources Research* **28**: 2925–2936.

Arcone SA, Lawson DE, Delaney AJ, Strasser JC, Strasser JD. 1998. Ground-penetrating radar reflection profiling of groundwater and bedrock in an area of discontinuous permafrost. *Geophysics* **63**: 1573–1584.

Best H, McNamara JP, Liberty L. 2005. Using ground-penetrating radar to investigate relationships between ice and hydraulic geometry in an arctic river. *Arctic, Antarctic, and Alpine Research* in press.

Buynevich IV, Fitzgerald DM. 2003. High-resolution subsurface (GPR) imaging and sedimentology of coastal ponds, Maine, U.S.A.: implications for Holocene back-barrier evolution. *Journal of Sedimentary Research* **73**: 559–571.

Cole KS, Cole RS. 1941. Dispersion and absorption in dielectrics, I, alternating current characteristics. *Journal of Chemical Physics* **9**: 341–351.

Davis JL, Scott WJ, Morey RM, Annan AP. 1976. Impulse radar experiments on permafrost near Tuktoyaktuk, Northwest Territories. *Canadian Journal of Earth Sciences* **13**: 1584–1590.

Delaney AJ, Arcone SA, Chacho Jr EF. 1990. Winter short-pulse radar studies on the Tanana River, Alaska. *Arctic* **43**: 244–250.

Dix CH. 1955. Seismic velocities from surface measurements. *Geophysics* **34**: 180–195.

Doolittle JA, Hardisky MA, Gross MF. 1990. A ground-penetrating radar study of active layer thicknesses in areas of moist sedge and wet sedge tundra near Bethel, Alaska, U.S.A. *Arctic and Alpine Research* **22**: 175–182.

Doolittle JA, Hardisky MA, Black S. 1992. A ground-penetrating radar study of Goodream Palsas, Newfoundland, Canada. *Arctic and Alpine Research* **24**: 173–178.

Edwardson KJ. 1997. *Characterizations of hyporheic influences on the hydrology and biogeochemistry of arctic tundra streams*. MS thesis, University of New Hampshire.

Edwardson KJ, Bowden WB, Dahm C, Morrice J. 2003. Transient storage and hyporheic transport in arctic tundra streams. *Advances in Water Resources* **26**: 907–923.

Greaves RJ, Lesmes DP, Lee JM, Toksoz MN. 1996. Velocity variation and water content estimated from multi-offset, ground-penetrating radar. *Geophysics* **61**: 683–695.

Haeni FP. 1996. Use of ground-penetrating radar and continuous seismic-reflection profiling on surface-water bodies in environmental and engineering studies. *Journal of Environmental and Engineering Geophysics* **1**: 27–35.

Hinkel KM, Doolittle JA, Bockheim JG, Nelson FE, Paetzold R, Kimble JM, Travis R. 2001. Detection of subsurface permafrost features with ground-penetrating radar, Barrow, Alaska. *Permafrost and Periglacial Processes* **12**: 170–190.

Hinzman LD, Kane DL, Gieck RE, Everett KR. 1991. Hydrologic and thermal properties of the active layer in the Alaskan Arctic. *Cold Regions Science and Technology* **19**: 95–110.

Kane DL, Hinzman LD, Woo MK, Everett KR. 1992. Arctic hydrology and climate change. In *Arctic Ecosystems in a Changing Climate, an Ecophysiological Perspective*. Chapin III FS, Jeffries RL, Reynolds JF, Shaver GR, Svoboda J (eds). Academic Press: New York.

Leibman MO. 1995. Preliminary results of cryogenic landslides study on Yamal Peninsula, Russia. *Permafrost and Periglacial Processes* **6**: 259–264.

McMichael CE, Hope AS, Stow DA, Fleming JB. 1997. The relation between active layer depth and a spectral vegetation index in arctic tundra landscapes of the North Slope of Alaska. *International Journal of Remote Sensing* **18**: 2371–2382.

McNamara JP, Kane DL, Hinzman LD. 1997. Hydrograph separations in an arctic watershed using mixing model and graphical techniques. *Water Resources Research* **33**(70): 1707–1720.

McNamara JP, Kane DL, Hinzman LD. 1998. An analysis of stream flow hydrology in an arctic drainage basin: a nested watershed approach. *Journal of Hydrology* **206**: 39–57.

Powers CJ, Haeni FP, Smith S. 1999. Integrated use of continuous seismic-reflection profiling and ground-penetrating radar methods at John's Pond, Cape Cod, Massachusetts. In *SAGEEP '99 Symposium on the Application of Geophysics to Environmental and Engineering Problems, Environmental and Engineering Geophysical Society, Proceedings*; 359–368.

Schwamborn GJ, Dix JK, Bull JM, Rachold V. 2002. High-resolution seismic and ground penetrating radar—geophysical profiling of a thermokarst lake in the western Lena delta, northern Siberia. *Permafrost and Periglacial Processes* **13**: 259–269.

Slater LD, Reeve A. 2002. Investigating peatland stratigraphy and hydrology using integrated electrical geophysics. *Geophysics* **67**: 365–378.

Stolt RH. 1978. Migration by Fourier transform. *Geophysics* **43**: 23–48.

Theimer BD, Nobes DC, Warner BG. 1994. A study of the geoelectric properties of peatlands and their influence on ground-penetrating radar surveying. *Geophysical Prospecting* **42**: 179–209.

Versteeg R, White EA, Rittger K. 2001. Ground penetrating radar and swept-frequency seismic imaging of shallow water sediments in the Hudson River. In *SAGEEP 2001, Environmental and Engineering Geophysical Society, Symposium on the Application of Geophysics to Environmental and Engineering Problems* (CDROM).

Yilmaz O. 2001. *Seismic Data Analysis*. Society of Exploration Geophysicists: Tulsa.

